Incoherent magnetization reversal in 30-nm Ni particles

C. A. Ross,[1,*] R. Chantrell,[2] M. Hwang,[1] M. Farhoud,[3] T. A. Savas,[4] Y. Hao,[1] Henry I. Smith,[3] F. M. Ross,[5] M. Redjdal,[6] and F. B. Humphrey[6]

[1]*Department of Materials Science and Engineering, Massachusetts Institute of Technology, Cambridge, Massachusetts 02139*

[2]*Department of Physics, University of Durham, Durham, DH1 3LE, United Kingdom*

[3]*Department of Electrical Engineering and Computer Science, Massachusetts Institute of Technology, Cambridge, Massachusetts 02139*

[4]*Department of Physics, Massachusetts Institute of Technology, Cambridge, Massachusetts 02139*

[5]*IBM T. J. Watson Research Center, Yorktown Heights, New York 10598*

[6]*Department of Electrical and Computer Engineering, Boston University, Boston, Massachusetts 02215*

(Received 20 March 2000; revised manuscript received 7 August 2000)

The magnetic properties of a 100-nm-period large-area array of regular, 30-nm polycrystalline nickel particles have been studied. The particles are found to reverse incoherently, and their hysteresis behavior has been compared with a computational model over a range of temperatures. Excellent agreement with the model is obtained, indicating that switching of the particles is dominated by the reversal of approximately 10-nm-diameter volumes within each particle. These switching volumes are identified with the columnar grains in the polycrystalline nickel, showing that the microstructure determines the magnetic behavior of the particles. This explains the anisotropy distribution and the onset of superparamagnetism in the sample. Incoherent reversal occurs even though the particles are only 1.5 times the exchange length in nickel, a size at which nearly uniform rotation is expected to occur if the particles were homogeneous.

I. INTRODUCTION

Ferromagnetic particles with dimensions of a few hundred nm and below show interesting magnetic behavior, and have applications in patterned magnetic media and other data storage systems.[1] In this size regime, the particles already show single-domain remanent states in which the magnetization is approximately parallel within the particle and there are no domain walls present. If the particles are large compared to the magnetic exchange length λ_{ex}, which is in the range 6–20 nm for ferromagnetic metals,[2] they are found to reverse by nonuniform (incoherent) processes[3–7] in which the switching field is considerably smaller than that predicted by the uniform (coherent) rotation model.[8] Here $\lambda_{ex}=\sqrt{A}/M_s$, where A is the exchange constant and M_s the saturation moment. However, as the particle size decreases, the switching field gradually increases, and the switching mode approaches uniform rotation for particle sizes much smaller than λ_{ex}, subject to thermal instability or ''superparamagnetic'' effects at finite temperature.[9,10] For storage and other applications, it is important to understand the factors that determine the reversal mechanism, the switching field, and the thermal stability of small particles, as a function of size. Lithographically produced arrays of identical particles are ideal for these studies in order to avoid variability in particle size and shape, or variability in spacing which leads to a spread in particle interactions.

There have been many observations of incoherent magnetization reversal in single particles or arrays of particles with dimensions of the order of 100 nm and above.[6,7,11–15] Data on smaller particles are less abundant, but low-temperature studies of a 25-nm Co particle,[16] 10–20-nm thick barium ferrite crystals,[17] and 10-nm diameter, 50–250-nm tall Fe pillars[18] have been presented. In each of these cases the particles are several times larger in some dimension than the exchange length. In the present work, we have evaluated the switching behavior and thermal stability of a regular array of weakly interacting, 30-nm diameter particles of nickel, for which $\lambda_{ex}=20\,\text{nm}$ (taking $A=10^{-6}\,\text{erg cm}^{-1}$), hence these particles are only 1.5 times λ_{ex} in their largest dimension. The regularity of the sample over large areas, and the small particle sizes compared to λ_{ex}, allow a detailed comparison to be made with the coherent rotation model over a large range of temperature.

We will show that, instead of following the coherent rotation model, reversal in these particles occurs within weakly coupled subunits, which we identify with the columnar grains of the polycrystalline nickel. We then model the hysteresis loops using a computational approach which gives values for the anisotropy and volume distributions of the reversing subunits. Some of the computational results were published elsewhere,[19] but in this work we relate the results to the particle microstructure, the results of a Landau-Lifschitz-Gilbert model, and the behavior of larger particles, to present a complete picture of reversal in these particles.

II. EXPERIMENTAL METHODS

Electron-beam lithography is most commonly employed for fabrication of features of sizes of 100 nm and smaller (e.g., Refs. 1, 12, 13, 20–22), but this method is slow and it is limited to the patterning of relatively small (submillimeter) areas of a substrate with very fine features. Instead, we have used interference lithography (IL) and achromatic interference lithography (AIL) combined with evaporation and lift-off to produce large areas of several square centimeters with uniform arrays of ferromagnetic particles of 100–200-nm period. Such samples have sufficient moment for characterization of their collective magnetic behavior using SQUID magnetometry or vibrating sample magnetometry (VSM).

IL was used to generate 200-nm period arrays, while AIL was used for 100-nm period arrays. Both methods rely on the interference of two laser beams to produce a standing wave which is used to expose a resist layer with a fringe pattern. Two perpendicular exposures are used to produce a template consisting of a square array of holes in a polymer layer, which was used to define the magnetic particles. In the case of IL[23–25] silicon substrates were coated with a trilayer resist stack consisting of layers of antireflective coating (ARC), evaporated silica, and Okha THMR-iN negative resist. The stack was exposed using a 351.1-nm wavelength laser, then the resist was developed to form a pattern of holes which was transferred into the silica then into the ARC using reactive ion etching (RIE). In the case of AIL,[26] fringe patterns were made by interference of a 193-nm wavelength laser in a trilevel stack that included a polymethyl methacrylate resist. A two-stage process was used to generate an array of holes in the ARC layer.[19,27] In both IL and AIL processes, the hole size was determined by the exposure dose and etching conditions, and was varied between about 30 and 90 % of the array period.

A film of nickel was deposited on the hole templates by electron-beam evaporation at a base pressure of 10^{-7} Torr and a deposition rate of 0.2 nm s^{-1}. Pyramid-shaped particles or truncated pyramids formed at the base of the holes because the holes closed off as the nickel film covered the top of the template. The template was then removed using a $H_2O_2/NH_4OH/H_2O$ solution to leave an array of nickel particles. Sample A, consisting of 100-nm period, 35-nm base, 40-nm height pyramids, sample B, truncated pyramids of 200-nm period, 80-nm base and 35-nm height, and sample C, which is approximately twice as large as A in period, base and height, are shown in Fig. 1. In sample A, pyramids were occasionally slightly displaced by the lift-off process, but this has negligible effects on their magnetostatic interactions. The dimensions and properties of the particles are summarized in Table I.

Hysteresis loops were measured both parallel and perpendicular to the plane of the substrate using SQUID magnetometry or VSM at a range of temperatures. The microstructure of the pyramids was investigated using x-ray diffraction with CuK_α radiation in θ-2θ geometry. The pyramid arrays contained too little nickel to produce measurable peaks, but scans on blanket films indicated a polycrystalline material with 10-nm grain size and with random or slightly (111)-preferred texture. The microstructure of the pyramids was explored further by transmission electron microscopy (TEM). To prepare samples, pyramids were scraped off the substrate using a blade and collected on a holey carbon grid. The adhesion of particles deposited directly onto silicon was too good to allow easy removal. However, if a gold layer were evaporated onto the substrate before lithography, the evaporated nickel adhered less well to the gold than to silicon, so the structures could be easily scraped off and imaged. Sample B was prepared in this way and images were taken with a JEOL 4000 TEM operated at 400 kV. At this voltage the evaporated structures are electron-transparent and could be imaged without thinning.

Figure 2 shows TEM images of sample B in plan view and cross section. A polycrystalline structure is evident, in agreement with the x-ray-diffraction data. Plan views show a range of grain diameters from a few nm to 15 nm, but in cross section it is seen that many of the nickel grains extend through the film thickness giving a columnar structure, with grain heights of 10–30 nm. An amorphous coating, assumed to be nickel oxide formed during the liftoff process or by exposure to the atmosphere, is visible surrounding the structures with a thickness of 3–4 nm. The grain size of the nickel in samples A and B is expected to be the same because the evaporation and liftoff processes were identical and the film thickness similar, but the grains in C will be on average taller and slightly wider because the film is thicker.

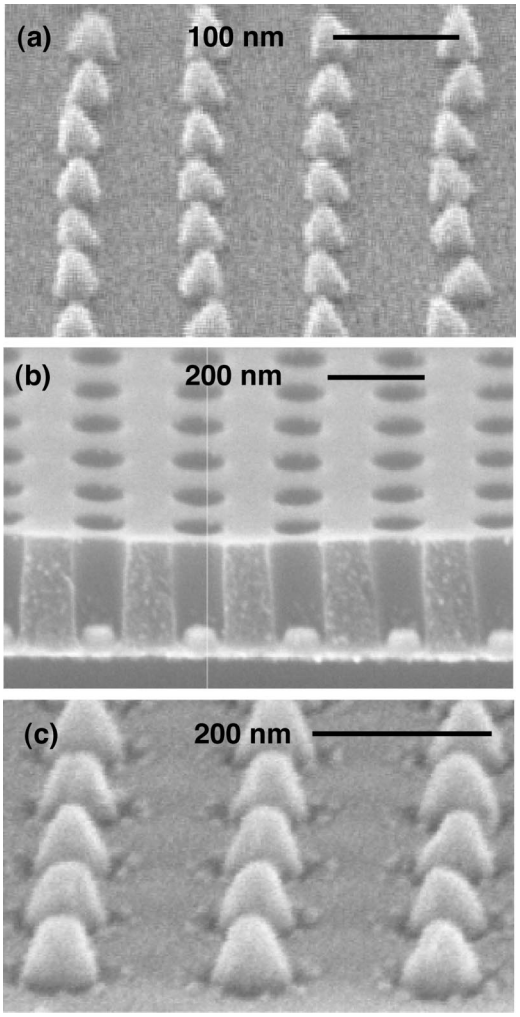

FIG. 1. Scanning electron micrographs of (a) sample A: 100-nm period, 35-nm base, 40-nm height pyramids. (b) Sample B: 200-nm period, 80-nm base, 35-nm height truncated pyramids, shown prior to removal (lift-off) of the template. The bright Ni particles are seen at the base of the holes in the template. (c) Sample C: 200-nm period, 90-nm base, 80-nm height pyramids.

III. MICROMAGNETIC CALCULATIONS

The behavior of individual *homogeneous* particles of nickel was calculated using a three-dimensional Landau-Lifschitz-Gilbert (LLG) micromagnetic model developed by Redjdal and Humphrey.[28] Particles were discretised into 1-nm cubes to approximate their shape. A pyramidal particle was modelled, consisting of a square base made of 31×31 elements and with a height of 35 elements, with an 11-nm

TABLE I. Dimensions and magnetic properties of samples A, B, and C.

Sample	Array period nm	Particle Base nm	Particle Height nm	Out-of-plane coercivity at 10 K, Oe	Out-of-plane coercivity at 300 K, Oe	In-plane coercivity at 10 K, Oe	In-plane coercivity at 300 K, Oe
A	100	35	40	570	20	120	10
B	200	80	35	243	72	246	61
C	200	89	80	630	300	150	50

Fitting parameters

Sample	V_m, nm^3	σ_v	K_m, erg cm^{-3}	σ_K	σ_θ
A	1000	0.6	1.8×10^5	0.7	0.6

wide truncated top, such that the angle between the base and the faces was 73.6°. The Landau-Lifschitz-Gilbert equations were solved for each cubic element subject to exchange coupling from its neighbors, magnetostatic coupling, and Zeeman energy from the applied field, using a 3D fast fourier transformation combined with zero padding to treat the isolated pyramidal shape. Magnetocrystalline anisotropy was neglected. The calculation uses an exchange constant of $A=10^{-6}$ erg cm^{-1}, a gyromagnetic ratio of $\gamma=0.0179$ Oe^{-1} ns^{-1}, and a damping coefficient of $\alpha=1$ to ensure a rapid convergence to the stable state at each value of applied field.

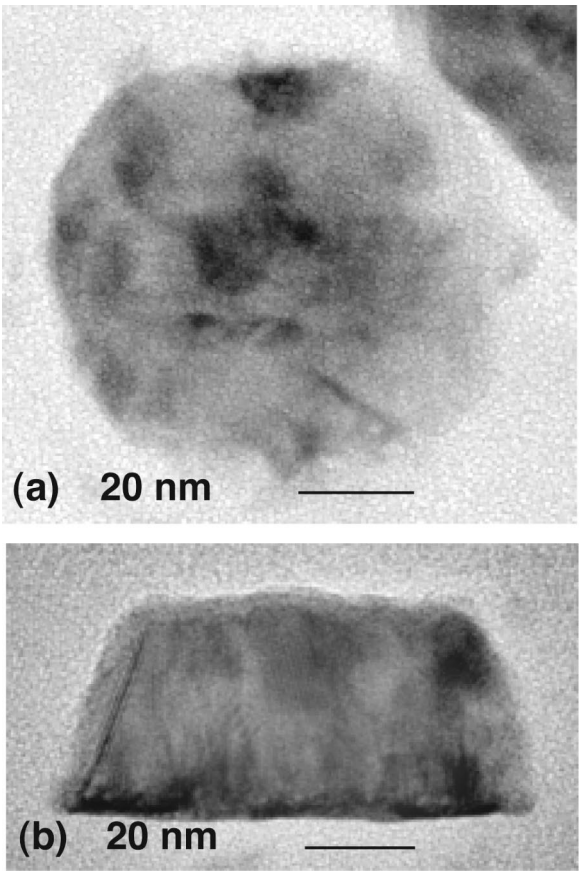

FIG. 2. Transmission electron micrographs of a particle from sample B, (a) plan view, (b) side view showing columnar grains and an amorphous oxide coating. The moire fringes in (b) are due to grains superposed in the beam direction.

The collective behavior of the arrays was calculated using a model of magnetostatically interacting coherently rotating particles subject to thermal fluctuations.[29] The particles in the model are placed on a square array and assigned volumes V from a lognormal distribution $p(x)$ with standard deviation σ_v and median V_m, such that

$$p(x)=[\sigma_v x\sqrt{(2\pi)}]^{-1}\exp-[(\ln x)^2/2\sigma_v^2], \qquad (1)$$

where $x=V/V_m$. Similarly, uniaxial anisotropies K follow a lognormal distribution with standard deviation σ_K and median K_m. The direction of the easy axes follows a sine-weighted Gaussian distribution with standard deviation σ_θ such that

$$p(\theta)=a\sin\theta\exp(-\sin^2\theta/2\sigma_\theta^2) \qquad (2)$$

in which the symmetry axis is perpendicular to the film plane, and a is a normalization constant. The particles were assigned the saturation moment M_s of pure Ni, 484 emu cm^{-3}. Interactions are calculated by summation over the nearest five neighbors plus a mean-field approach for the remainder of the material. The model consists of two phases: thermally stable particles and superparamagnetic particles, which are treated using different approaches but which are coupled magnetostatically. Each particle is treated as a classical spin of moment M_sV which transitions between two energy minima separated by barrier ΔE with probability $p=1-\exp(-t_m/\tau)$, where t_m is the measurement time and τ the relaxation time given by $\exp(-\Delta E/kT)$. ΔE is calculated numerically.[30] When p is high, the particles behave superparamagnetically, and standard Monte Carlo (MC) moves ensure that the particles reach equilibrium. When p is low, transitions were determined by comparing p with a random number. For moments able to make the transition, MC moves carried out between the minima ensure the correct Boltzmann distribution, then MC moves about the minimum ensure that local equilibrium is reached. At least 100 MC steps were carried out at each field.

The five parameters V_m, σ_v, K_m, σ_K, and σ_θ, are adjusted to fit the hysteresis loops to the measured data at different temperatures (10 to 300 K) and for different directions of the applied field (in plane and out of plane). The same

values for the parameters are used to fit each data set. Although there are five parameters in this model, each one affects the hysteresis loop shape differently. The fit for the particle size parameters V_m and σ_v is unique because the variation of coercivity with temperature is very sensitive to particle size, with the high temperature tail accurately determining the standard deviation. The value of K_m is determined very accurately by the low temperature coercivity. The orientation function for the anisotropy axes is itself determined accurately by the difference between the in-plane and out-of-plane data. The one parameter which is defined less accurately is the width of the anisotropy distribution σ_K. This has its largest effect on the approach to saturation of the hysteresis loops. The fit is indicative of the width of the anisotropy distribution rather than being extremely sensitive to the functional form of the distribution. As will be seen below, the good quality of the fit to the hysteresis loop shapes and to their temperature dependence gives an excellent determination of V_m, σ_v, K_m, and σ_θ, with σ_K being determined less precisely.

IV. EXPERIMENTAL RESULTS

Although the measured saturation moment M_s of blanket films of nickel was close to that of pure nickel, indicating that the as-deposited material had a high purity, pyramid arrays typically showed a lower saturation moment than expected from their volume. This is due to oxidation of their surfaces, as was indicated by TEM in sample B. For example, the moment of sample A was 3.6×10^{-5} emu cm^{-2}, which is consistent with the outer 4–5 nm of each pyramid being composed of nonmagnetic material while the interior consists of pure Ni, approximately 26-nm base and 32-nm high.

Nickel oxide is an antiferromagnet, but we found that the surface oxide had negligible effects on the magnetic behavior of the particles except at low temperature. Evidence of antiferromagnetic coupling was seen only at 10 K, in which the field-cooled hysteresis loop showed an offset of 150 Oe. This was verified in two separate measurements. However, at 50 K and higher there was no offset. It is likely that the Néel temperature of the oxide is low compared to that of crystalline NiO because the oxide has very poor structural order, as indicated by TEM. The loop offset at 10 K was subtracted prior to fitting the data to the model.

Figure 3 shows in-plane and out-of-plane hysteresis loops for sample *A* measured at various temperatures. The coercivity both in-plane and out-of-plane was small at room temperature, and the sample had very little hysteresis, but at low temperatures an easy axis clearly exists perpendicular to the film plane, and the coercivity increased to 570 Oe. Figure 4 shows the variation of coercivity with temperature in more detail.

As a comparison, magnetic data for sample C are shown in Fig. 5. This sample has similar particle shape to A but its period, width and height are twice as large. Sample C has an out-of-plane anisotropy and similarly shaped hysteresis loops to those of sample A, but its coercivity is 650 Oe at 10 K and 350 Oe at room temperature. The low temperature coercivity is higher than that of A, showing that the anisotropy *K* of the particles in sample C is higher than that of A. Also, the slower decrease in coercivity with temperature for C indicates that the product *KV* of anisotropy and switching volume is larger for sample C than for sample A.

V. COMPUTATIONAL RESULTS

We performed a micromagnetic calculation of the remanent state and switching behavior of a homogeneous nickel particle of the same dimensions as sample A using the LLG model. Figure 6(a) shows the remanent state after saturation with a field along the axis and Fig. 6(b) shows the remanent state after saturation parallel to the base plane. In each case the pyramid has remanence of 1.0, and the magnetization is almost uniform within the particle, with slight deviations at the corners and edges. This behavior arises because the particle is not much larger than λ_{ex} and has very little shape anisotropy due to its similar height and base dimensions. Figure 6(c) shows a sequence of magnetization states during reversal which indicate that the model particle switches by a nearly uniform rotation process, with a reversal volume equal to the physical particle volume.

The results indicate that a homogeneous nickel particle of these dimensions would show little anisotropy, hence a low switching field at all temperatures, and near uniform reversal behavior. This is in contrast to the measured data that show a high out-of-plane anisotropy at low temperatures and a hard axis parallel to the sample plane. We believe that the nonuniform switching behavior is due to the microstructure of the pyramid. In order to investigate this further we modelled the hysteresis loops using the collective magnetic model described in Sec. III. A single set of fitting parameters (Table I) was chosen to give the best fit over the entire temperature range. The results of the fits to the hysteresis loops are shown in Fig. 3, and the variation of coercivity with temperature is shown in Fig. 4.

The fits at all temperatures, and for in-plane and out-of-plane field directions, give the following set of fitting parameters: $V_m=1000$ nm^3, $\sigma_v=0.6$, $K_m=1.8\times10^5$ erg cm^{-3}, $\sigma_K=0.7$ and $\sigma_\theta=0.6$. The particles were very weakly interacting, which was evident from the model results and from the geometry of the array, in which the nearest neighbor interaction field was only 2 Oe. It is immediately apparent that the magnetic volume V_m is considerably smaller than the 6000 nm^3 physical volume of the particles, and has a wide size distribution σ_v. Additionally, the median anisotropy K_m is greater than the room temperature magnetocrystalline anisotropy of pure nickel for which $K_1=5\ 10^4$ erg cm^{-3}, and has a wide distribution in magnitude, σ_K and direction σ_θ. The distribution of V, K, and θ is shown in Fig. 7.

The variation of coercivity with temperature, seen in Fig. 4, is indicative of the distribution of sizes characterized by σ_v. An assembly of noninteracting, identical, aligned uniaxial nickel particles with volume V_m and anisotropy K_m would have zero coercivity above a blocking temperature of $T_b=K_mV_m/25k=52$ K, and the coercivity would increase below T_b according to $H_K\ [1-(T/T_b)^{0.5}]$ where $H_K=2K_m/M_s=750$ Oe.[31] In contrast, in the sample, the spread in K and V leads to a range in T_b, and the existence of a finite coercivity at room temperature is instead due to the presence of the small number of larger volumes within the distribution.

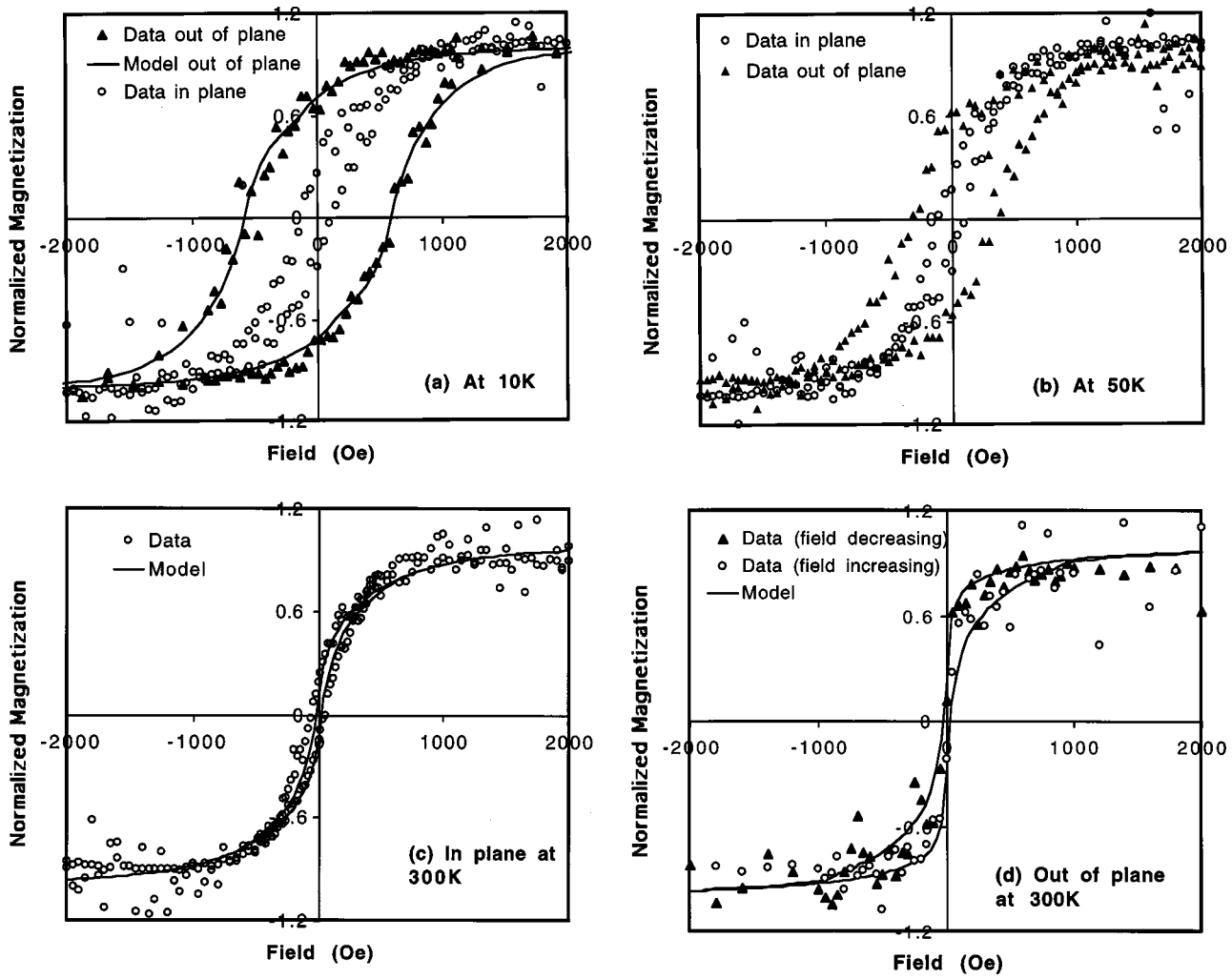

FIG. 3. Magnetic hysteresis loops from sample A (a) out-of-plane with fit and in plane at 10 K. An offset of 150 Oe was subtracted from the out-of-plane loop prior to fitting. (b) Hysteresis loops at 50 K, (c) In plane hysteresis loop at 300 K with fit, (d) out-of-plane loop at 300 K with fit. Magnetization is normalized to 3.6×10^{-5} emu cm^{-2}.

VI. DISCUSSION

We have seen that the particles in sample A do not reverse by coherent rotation, and the fit to the collective model shows that reversal occurs within a volume smaller than the physical volume of the particle. The volume distribution V determined from the collective model peaks for volumes in the range of ~400–1400 nm^3, which coincides with the volumes of the majority of the grains in the pyramids. We propose that the switching is dominated by the reversal of indi-

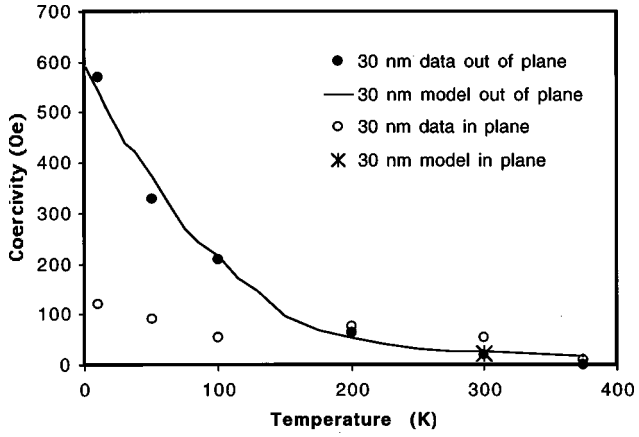

FIG. 4. Variation of coercivity with temperature for sample A, with fit from the model.

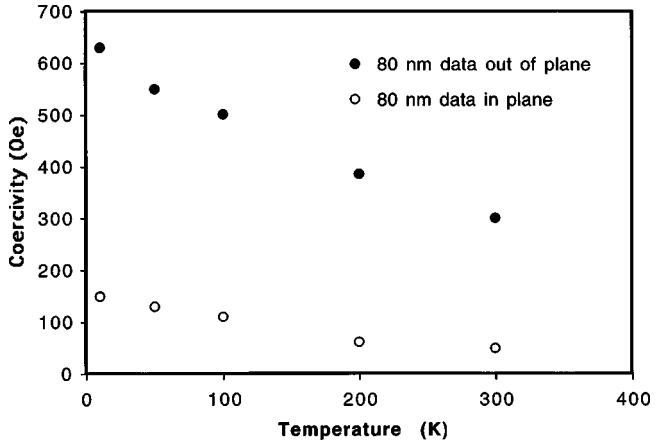

FIG. 5. Variation of coercivity with temperature for sample C, for comparison with Fig. 4.

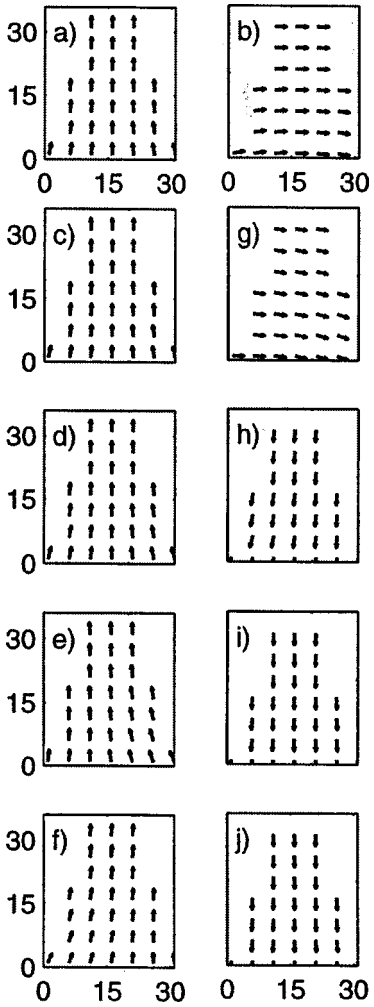

FIG. 6. Micromagnetic calculation of a 31×31-nm base, 35-nm high nickel pyramid. A subset of the magnetization vectors is shown for clarity. (a) remanent state after magnetization parallel to axis, z (scale is in nm); (b) remanent state after magnetization parallel to the base, x; (c)–(j) sequence of magnetization states when a -2000 Oe field is applied parallel to the axis, based on a damping coefficient of $\alpha=1$. The nearly uniform switching event occurs in frame (g).

vidual grains within the pyramid. The large standard deviations in volume, anisotropy, and angular distribution, despite the physical regularity of the array, are also consistent with reversal originating within individual grains. K_m is four times larger than the magnetocrystalline anisotropy of nickel, and the array has a pronounced out-of-plane anisotropy at low temperatures. This implies that shape anisotropy is the dominant contribution to K, and that the switching volumes are elongated along the film normal. Although the magnetocrystalline anisotropy of nickel increases at low temperatures, this alone would not give the observed perpendicular anisotropy because the grains are randomly oriented. It should be noted that the model treats the distributions of K and V as independent. In our interpretation, K and V are related through the shape of the switching volume because K is the shape anisotropy corresponding to the volume V. An ellipsoidal nickel particle of aspect ratio 1.4 would have a shape anisotropy of 1.8×10^5 erg cm^{-3}, so only modest elongation is required, which is consistent with the columnar

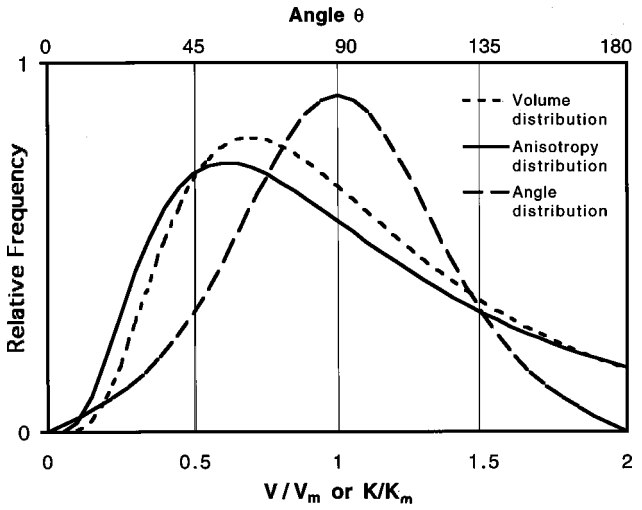

FIG. 7. Distribution of volumes and anisotropies from Eqs. (1) and (2) based on the best fit parameters from the model for sample A.

grain shapes seen in TEM. Magnetostriction is not expected to contribute to anisotropy because any residual strain would be substantially relaxed in particles of this aspect ratio.

This interpretation of reversal originating within grains comprising the particles is consistent with the differences observed between samples A and C. In C, the grains are taller on average because the film is thicker, leading to a higher shape anisotropy and grain volume than in A. We expect that the grains inside each pyramid have some exchange coupling, and the reversal of one grain leads to reversal of the entire pyramid. The net anisotropy of a nickel particle therefore depends on the shape of its grains as well as on its overall shape. Evidence of microstructurally induced perpendicular anisotropy in evaporated nickel has been found by other authors,[32,33,22] and by ourselves.[34] In the latter work, we compared the remanence of 80–120 nm evaporated nickel particles to the results of micromagnetic calculations, and the data implied the existence of perpendicular anisotropy in the range $5\times10^4-2\times10^5$ erg cm^{-3}.

These results have interesting implications for the design of patterned media and other devices that use small polycrystalline ferromagnetic particles. It is commonly assumed that uniform rotation describes the magnetic behavior and thermal stability of small particles close to the magnetic exchange length. However, we have shown that even particles of $1.5\lambda_{ex}$ show nonuniform magnetization behavior and a much greater vulnerability to superparamagnetism than is expected from the uniform rotation of the particle, due to the internal grain structure. Other inhomogeneities such as surface oxidation[35] or roughness[22,36,37] may also contribute to nonuniform reversal in small particles. Most importantly, there is a wide spread in the anisotropy and switching volume of such particles, giving a wide range of switching fields of apparently identical particles, which presents a problem in applications such as patterned media and MRAM devices. Indeed, many authors have found significant variations in the behavior of nominally identical (though larger) lithographically patterned particles.[12–14,21,32,38,39] Thus to make devices based on small, discrete magnetic particles, it is necessary to control not only the lithographic processing but the micro-

structure (grain size, shape and orientation, surface structure, and intergranular coupling) of the magnetic material.

CONCLUSIONS

30-nm pyramids of nickel show clear evidence of incoherent reversal, despite their size being only 1.5 times the exchange length in nickel, a size at which uniform rotation would be predicted in a homogeneous particle. The high anisotropy at low temperatures, the size dependence of the magnetic properties, and the columnar microstructure revealed by TEM, suggest that reversal is initiated within the grains that comprise the particles. The particles show excellent quantitative agreement with a computational model over a range of temperatures and field directions, which reveals that switching occurs in approximately 10-nm-diameter volumes which possess shape anisotropy perpendicular to the film plane. These switching volumes are identified with the individual columnar grains within the pyramids, and are small enough to lead to superparamagnetic behavior at room temperature. The importance of the microstructure in the reversal process may be responsible for the wide spread in switching fields which is frequently observed in apparently identical particles. This has major implications in the design of magnetic nanoelements for data storage and other applications.

ACKNOWLEDGMENTS

The authors gratefully acknowledge support from NSF DMR-9871539, IBM for M.F., and the UK EPSRC, and thank L. Gignac for use of TEM facilities at IBM.

*Email address: caross@mit.edu

[1] S. Y. Chou, Proc. IEEE **85**, 652 (1997).
[2] M. Schabes, J. Magn. Magn. Mater. **95**, 249 (1991).
[3] D. R. Fredkin and T. R. Koehler, J. Appl. Phys. **67**, 5544 (1990).
[4] H. L. Richards, S. W. Sides, M. A. Novotny, and P. A. Rikvold, J. Magn. Magn. Mater. **150**, 37 (1995).
[5] A. Aharoni, J. Appl. Phys. **82**, 1281 (1997).
[6] R. O'Barr and S. Schultz, J. Appl. Phys. **81**, 5458 (1997).
[7] C. Seberino and H. N. Bertram, IEEE Trans. Magn. **33**, 3055 (1997).
[8] E. C. Stoner and E. P. Wohlfarth, Philos. Trans. R. Soc. London, Ser. A **240**, 599 (1948).
[9] L. Neel, Ann. Geophys. **5**, 99 (1949).
[10] W. F. Brown, Phys. Rev. **130**, 1677 (1963).
[11] M. Lederman, G. A. Gibson, and S. Schultz, J. Appl. Phys. **73**, 6961 (1993); M. Lederman, S. Schultz, and M. Ozaki, Phys. Rev. Lett. **73**, 1986 (1994).
[12] W. Wernsdorfer, K. Hasselbach, A. Sulpice, A. Benoit, J. E. Wegrowe, L. Thomas, B. Barbara, and D. Mailly, Phys. Rev. B **53**, 3341 (1996).
[13] M. Kleiber, F. Kummerlen, M. Lohndorf, A. Wadas, D. Weiss, and R. Wiesendanger, Phys. Rev. B **58**, 5563 (1998).
[14] J. E. Wegrowe, O. Fruchart, J.-P. Nozieres, D. Givord, F. Rousseaux, D. Decanini, and J. Ph. Ansermet, J. Appl. Phys. **86**, 1028 (1999).
[15] O. Fruchart, J-P. Nozieres, W. Wernsdorfer, D. Givord, F. Rousseaux, and D. Decanini, Phys. Rev. Lett. **82**, 1305 (1999).
[16] W. Wernsdorfer, E. Bonet Orozco, K. Hasselbach, A. Benoit, B. Barbara, N. Demoncy, A. Loiseau, H. Pascard, and D. Mailly, Phys. Rev. Lett. **78**, 1791 (1997).
[17] W. Wernsdorfer, E. Bonet Orozco, K. Hasselbach, A. Benoit, D. Mailly, A. Thiaville, O. Kubo, H. Nakano, and B. Barbara, Phys. Rev. Lett. **97**, 4014 (1997); E. Bonet, W. Wernsdorfer, B. Barbara, A. Benoit, D. Mailly, and A. Thiaville, *ibid.* **99**, 4188 (1999).
[18] S. Wirth, M. Field, D. D. Awschalom, and S. von Molnar, Phys. Rev. B **57**, R14 028 (1998); S. Wirth, S. von Molnar, M. Field, and D. D. Awschalom, J. Appl. Phys. **85**, 5249 (1999).
[19] C. A. Ross, T. A. Savas, H. I. Smith, M. Hwang, and R. Chantrell, IEEE Trans. Magn. **35**, 3781 (1999).
[20] J. F. Smyth, S. Schultz, D. Fredkin, D. P. Kern, S. A. Rishton, H. Schmid, M. Cali, and T. R. Koehler, J. Appl. Phys. **69**, 5262 (1991).
[21] C. Haginoya, S. Heike, M. Ishibashi, K. Nakamura, K. Koike, T. Yoshimura, J. Yamamoto, and Y. Hirayama, J. Appl. Phys. **85**, 8327 (1999).
[22] R. P. Cowburn, J. Phys. D **33**, R1 (2000).
[23] M. L. Schattenberg, R. J. Aucoin, and R. C. Fleming, J. Vac. Sci. Technol. B **13**, 3007 (1995).
[24] C. A. Ross, H. I. Smith, T. A. Savas, M. Schattenburg, M. Farhoud, M. Hwang, M. Walsh, M. C. Abraham, and R. J. Ram, J. Vac. Sci. Technol. B **17**, 3168 (1999).
[25] M. Farhoud, H. I. Smith, M. Hwang, and C. A. Ross, J. Appl. Phys. (to be published).
[26] T. A. Savas, M. L. Schattenburg, J. M. Carter, and H. I. Smith, J. Vac. Sci. Technol. B **14**, 4167 (1996).
[27] T. A. Savas, M. Farhoud, H. I. Smith, M. Hwang, and C. A. Ross, J. Appl. Phys. **85**, 6160 (1999).
[28] M. Redjdal and F. B. Humphrey, J. Appl. Phys. **79**, 6464 (1996).
[29] M. El-Hilo, R. W. Chantrell, and K. O'Grady, J. Appl. Phys. **84**, 5114 (1998).
[30] H. Pfeiffer, Phys. Status Solidi B **118**, 295 (1990).
[31] B. D. Cullity, *Introduction to Magnetic Materials* (Addison-Wesley, Reading, MA, 1972).
[32] G. Meier and M. Kleiber, Appl. Phys. Lett. **72**, 2168 (1998).
[33] G. Skidmore. Ph.D. thesis, U. Minnesota, 1997.
[34] C. A. Ross, M. Farhoud, M. Hwang, Henry I. Smith, M. Redjdal, and F. B. Humphrey, J. Appl. Phys. (to be published).
[35] R. H. Kodama, A. E. Berkowitz, E. J. McNiff, and S. Foner, Phys. Rev. Lett. **77**, 394 (1996).
[36] J. Gadbois and J. G. Zhu, IEEE Trans. Magn. **31**, 3802 (1995).
[37] T. Schrefl, J. Fidler, K. J. Kirk, and J. N. Chapman, J. Appl. Phys. **85**, 6169 (1999).
[38] R. M. H. New, R. F. W. Pease, and R. L. White, IEEE Trans. Magn. **31**, 3805 (1995).
[39] Y. Zheng and J.-G. Zhu, J. Appl. Phys. **81**, 5471 (1997).